

Thermoplasmonics with Gold Nanoparticles: A New Weapon in Modern Optics and Biomedicine

Alexa Guglielmelli, Filippo Pierini, Nelson Tabiryan, Cesare Umeton, Timothy J. Bunning, and Luciano De Sio*

Thermoplasmonics deals with the generation and manipulation of nanoscale heating associated with noble metallic nanoparticles. To this end, gold nanoparticles (AuNPs) are unique nanomaterials with the intrinsic capability to generate a nanoscale confined light-triggered thermal effect. This phenomenon is produced under the excitation of a suitable light of a wavelength that matches the localized surface plasmonic resonance frequency of AuNPs. Liquid crystals (LCs) and hydrogels are temperature-sensitive materials that can detect the host AuNPs and their photo-induced temperature variations. In this perspective, new insight into thermoplasmonics, by describing a series of methodologies for monitoring, detecting, and exploiting the photothermal properties of AuNPs, is offered. From conventional infrared thermography to highly sophisticated temperature-sensitive materials such as LCs and hydrogels, a new scenario in thermoplasmonic-based, next generation, photonic components is presented and discussed. Moreover, a new road in thermoplasmonic-driven biomedical applications, by describing compelling and innovative health technologies such as on-demand drug-release and smart face masks with smart nano-assisted destruction of pathogens, is proposed. The latter represents a new weapon in the fight against COVID-19.

1. Introduction


In the past years, gold nanoparticles (AuNPs) have been extensively utilized in several research fields thanks to their optical and thermo-optical properties.^[1] AuNPs possess the capability to focus a strong electromagnetic field at the nanoscale level thanks to a physical phenomenon named localized surface plasmon resonance (LSPR). LSPR is associated with the coherent and dipolar oscillation of the free electrons localized at the metal/dielectric interface.^[2] When the AuNP surface is illuminated with a suitable (resonant) light source, the LSPR oscillation produces a strong temperature increase, thus turning the AuNP into a localized nanosource of heat. The absorption of light by AuNPs and the following heat generation has long been considered only a side effect, to avoid or to be minimized,^[3] and efforts have been channeled toward the compensation of dissipative losses in plasmonic materials.^[4]

After the first demonstration of AuNP-based plasmonic photothermal therapy (PPTT) for cancer in 2003 by Halas and co-workers,^[5] the opinion concerning

Dr. A. Guglielmelli
Department of Physics
University of Calabria
87036 Arcavacata di Rende, Cosenza, Italy

Dr. A. Guglielmelli, Dr. L. De Sio
CNR-Lab. Licryl
Institute NANOTEC
Arcavacata di Rende 87036, Italy
E-mail: luciano.desio@uniroma1.it

Prof. F. Pierini
Department of Biosystems and Soft Matter
Institute of Fundamental Technological Research
Polish Academy of Sciences
Warsaw 02-106, Poland

 The ORCID identification number(s) for the author(s) of this article can be found under <https://doi.org/10.1002/adpr.202000198>.

© 2021 The Authors. Advanced Photonics Research published by Wiley-VCH GmbH. This is an open access article under the terms of the Creative Commons Attribution License, which permits use, distribution and reproduction in any medium, provided the original work is properly cited.

DOI: 10.1002/adpr.202000198

Dr. N. Tabiryan
Beam Engineering for Advanced Measurements Company
Orlando, FL 32810, USA

Prof. C. Umeton
Department of Physics
University of Calabria
87036 Arcavacata di Rende, Cosenza, Italy

Dr. T. J. Bunning
Materials and Manufacturing Directorate
Air Force Research Laboratory
Wright-Patterson Air Force Base, OH 45433-7707, USA

Dr. L. De Sio
Department of Medico-Surgical Sciences and Biotechnologies
Center for Biophotonics
Sapienza University of Rome
Corso della Repubblica 79, 04100 Latina, Italy

AuNPs as nanosources of heat completely changed, turning the material losses into performance gain, opening new opportunities in thermal-based modern applications. Since then, numerous studies have been carried out to push the initial proposal toward clinical trials.^[6] Indeed, it was more than clear that to heat the local environment and destroy cancer cells, the strong LSPR absorption, followed by fast energy conversion and dissipation, could be exploited readily by using light radiation with a frequency strongly overlapping with the AuNPs LSPR band.^[6a] This effect is on the basis of PPTT and represents a potentially favorable alternative to traditional treatments of localized tumors such as chemotherapy, radiotherapy, and surgery. Nowadays, the photothermal properties of AuNPs are widely used not only for cancerous cells and tumors^[7] but also for selective destruction of antibiotic-resistant bacteria,^[8] and the treatment of HIV.^[9] A very recent application of thermoplasmonics has been also employed in the battle against coronavirus outbreak. Some examples are mainly devoted to detecting the current pandemic (SARS-CoV-2), enabling a real-time and label-free detection of viral sequences;^[10] other applications are aimed at realizing nano-based antimicrobial and antiviral formulations that are not only suitable for disinfecting air and surfaces but are also effective in reinforcing personal protective equipment such as facial respirators.^[11] Other emerging applications of thermoplasmonics are also present in nonbiomedical field, such as energy,^[12] solar and thermal energy harvesting,^[13] nanofluidics,^[14] nanofabrication,^[15] nanomanipulation,^[16] heat-assisted magnetic recording (HAMR) for data storage,^[17] photonics, and optoelectronics.^[18] In the most disparate fields, all these applications have given rise to the real need to monitor the heat-induced by the photothermal effect at the nanoscale and the macroscale, generated by an ensemble of AuNPs. The detection of the temperature change in the proximity of the AuNP surface is a crucial application. One technique relies on the utilization of temperature-sensitive materials as media surrounding the AuNP. As such, it can be made by embedding AuNPs in ice^[19] or using photothermal optical probes,^[20] based, for example, on thermoresponsive molecules such as thermotropic liquid crystals (LCs)^[21] or biologically relevant molecules such as DNA,^[22] where the thermal response of the smart material is known. As for nanoscale temperature monitoring, the collective heating from irradiated NPs immersed in colloidal solutions or deposited on a substrate can be readily monitored by means of bulk measurements by using several methods, like thermal imaging^[23] or a simple thermometer. Herein, we report on the photothermal properties of AuNPs both from a theoretical and experimental point of view. We analyze the main methodologies utilized for monitoring and measuring the nanolocalized temperature increase. We track down a new opportunity in thermoplasmonics by exploiting the different applications ranging from innovative optical components to advanced medical applications.

2. Fundamentals of Localized Plasmon Resonance in Gold Nanoparticles

Gold has always aroused a strong interest for its unique chemical and optical properties, both in its macroscopic and microscopic state. The most exciting phenomena emerge in the metal

structures down to sizes of the order of a few nanometers. The behavior of the matter at the nanoscale is unexpected and different from the bulks one. It is related to the unusual electronic configuration combined with other effects due to the tiny dimensions. AuNPs have a considerable number of free conduction and easily polarizable electrons, predominantly distributed at the surface, an essential prerequisite for interacting with electromagnetic (EM) fields. The main consequence is that the AuNPs are capable of squeezing EM waves into tiny scales. Indeed, under the influence of an external EM field, the free electrons of the AuNP start to oscillate in phase with the EM field, and the frequency associated with this oscillation is called plasmon resonance ω_{LSPR} . Consequently, the external EM field's electric component induces a force on the conductive electrons, thus displacing them from their intrinsic equilibrium state with consequent unbalanced charges at the AuNP surface. The resulting difference in the total charge at the AuNPs surface behaves as a restoring force, causing a dipolar oscillation of all electrons with the same phase. Hence, an NP's plasmon can be seen as a light-activated harmonic oscillator. The electron cloud oscillates like a simple dipole parallel to the electric field of the EM radiation (Figure 1).

From a theoretical point of view, for an isolated spherical AuNP with a size much smaller than the wavelength of visible light ($a \ll \lambda$), in the quasi-static approximation regime, the displacement of the electron cloud relative to the core atoms, in response to $\vec{E}(\vec{r}, \omega)$, can be expressed by the metal polarizability $\vec{P}(\vec{r}, \omega)$. When the NP involved in the optical process is a subwavelength AuNP, the interaction with the EM field can be investigated by using the simple quasi-static approximation.^[24] However, for larger AuNPs (starting from 30 nm diameter), this dipolar approximation is no more accurate because significant higher order multipolar modes emerge, and more complex models, such as Mie theory^[2,25] are required, which can account for retardation effects. First of all, to quantify the scattered/absorbed radiation, implementing a theoretical model is necessary to consider the wave nature of light. Indeed, the interaction between a suitable light source and an NP produces absorption (absorption cross-section, σ_{abs}) and scattering (scattering cross-section, σ_{sca}) of the incident radiation, thus generating a light attenuation characterized by an extinction cross-section (σ_{ext}). For small AuNPs ($a \ll \lambda$) σ_{ext} strictly depends on the absorption process: $\sigma_{\text{sca}} \ll \sigma_{\text{abs}} \approx \sigma_{\text{ext}}$, and is defined as follows

$$\sigma_{\text{ext}} = 9 \frac{\omega}{c} \varepsilon_m^{3/2} V \frac{\varepsilon_2}{[\varepsilon_1 + 2\varepsilon_m]^2 + \varepsilon_2^2} \quad (1)$$

where $\varepsilon(\omega) = \varepsilon_1(\omega) + i\varepsilon_2(\omega)$ is the dielectric function of the metal, ε_m is the dielectric constant of the surrounding medium, and $V = \frac{4}{3}\pi a^3$ is the AuNP volume. It is evident that σ_{ext} undergoes a resonant amplification, reaching its maximum value when the denominator quantity $|\varepsilon + 2\varepsilon_m|$ is minimum, that is the called Fröhlich condition. Furthermore, from Equation (1), it is noticeable that: 1) the optical properties of the material depend on its $\varepsilon(\omega)$; 2) σ_{ext} is directly proportional to the volume of the AuNP; 3) the Fröhlich condition, via the ε_m , defines the LSPR position. The LSPR frequency control can be obtained by varying the AuNP surrounding medium, $\varepsilon_m(\omega)$, size, shape, and composition. Richard Gans further extended the Mie theory to include

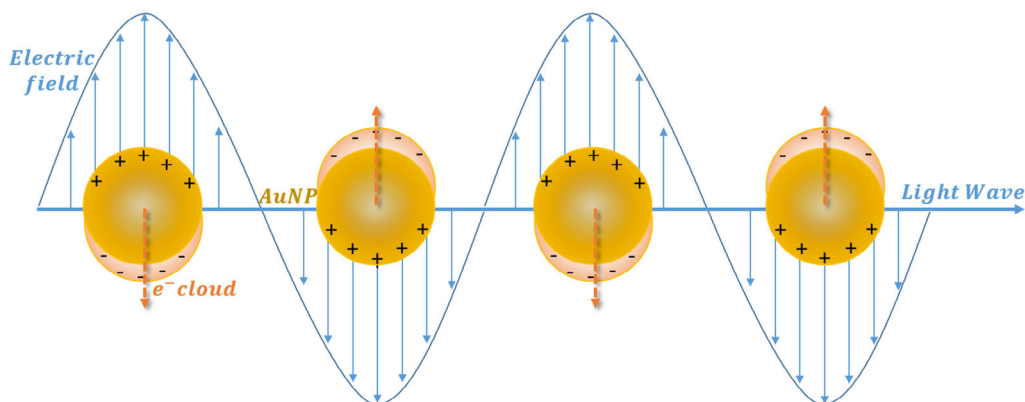


Figure 1. Scheme of a surface plasmon oscillation for a spherical AuNP, showing the displacement of the conduction electron charge cloud relative to the nuclei.

spheroidal AuNPs of any aspect ratio in the small AuNP approximation. In Gans theory, the absorption is mainly related to the aspect ratio (AR) of the AuNPs and not to the absolute dimensions. In this framework, the σ_{ext} for a prolate spheroid (rod-shaped AuNP) is found analogous to that one of the spherical AuNPs, as^[25b]

$$\sigma_{\text{ext}} = \frac{\omega}{3c} \epsilon_m^{3/2} V \sum_j \frac{(1/P_j^2) \epsilon_2}{[\epsilon_1 + [(1 - P_j)/P_j] \epsilon_m]^2 + \epsilon_2^2} \quad (2)$$

The depolarization factors (P_j) along the axes are described in terms of the AR and eccentricity e .

3. Physics of Plasmonic Heating

The LSPR is an efficient way to confine energy into the extremely small volume of an AuNP, thus drastically enhancing both its absorption and scattering cross-sections.^[26] While the scattering cross-section tells how much energy is reradiated by the AuNP in the form of light, the absorption cross-section specifies the portion of absorbed light that is re-emitted in the form of heat. Thus, absorption is what primarily matters in thermoplasmonics.^[27] Taking advantage of this light-to-heat conversion provides access to an innovative way of studying and controlling heat-induced

phenomena at the nanoscale. To get a deeper insight into these processes, it is necessary to take into account that the optical properties of the nano-objects under investigation are governed by a series of energy exchanges, each of them characterized by a typical time scale (Figure 2).^[26]

In the interaction with an impinging short light pulse in the visible spectral domain, the AuNPs can gain energy by absorbing photons through electron transitions. If the frequency of the incident radiation matches the LSPR band, a resonant coupling with the EM wave occurs, with a resulting excitation at the plasmon resonance (Figure 2a); this triggering of phenomena appears as a collective, coherent, and dipolar oscillation of electrons of the conduction band. The result is a global nonequilibrium condition. To restore the internal thermal equilibrium of these electrons, the energy is redistributed, through electron–electron collisions (e–e), inside the quasi-free electronic gas. This process occurs on a time scale of approximately $10 \text{ fs} \leq \tau \leq 100 \text{ fs}$. Subsequently, the hot carriers' energy is redistributed with a relaxation process (Figure 2b) through the scattering associated with the electron–phonon-interaction (e–ph) in a time interval of $100 \text{ fs} \leq \tau \leq 1 \text{ ps}$. The last step takes into account the medium surrounding the AuNP, and the transfer of thermal energy to the interface, via phonon–phonon-collisions (ph–ph), on a $10 \text{ ps} \leq \tau \leq 10 \text{ ns}$ time scale. This last process (thermal dissipation, Figure 2c) leads to the cooling of the AuNP, which releases heat to the surrounding

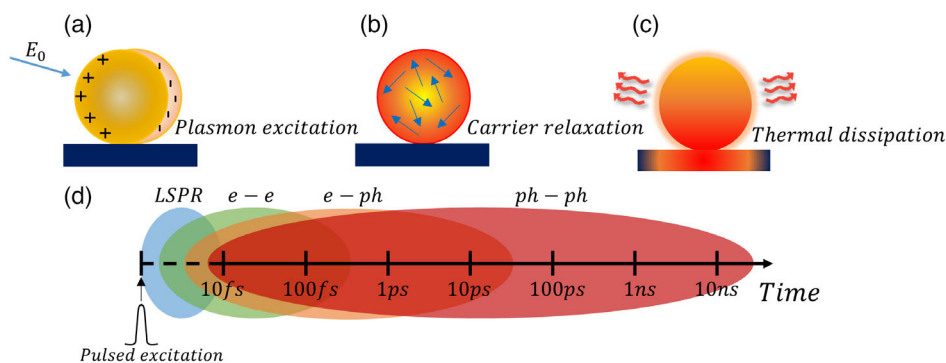


Figure 2. a) Schematic illustration of photoexcitation of LSPR, b) relaxation of photoexcited LSPR, c) releases of thermal energy to the surrounding medium, d) energy exchanges involved in the photothermal response of AuNPs on a logarithmic time scale.

medium, causing its temperature to rise. The dynamics of this process (see in the following paragraphs) strongly depends on the heat transfer properties of the surrounding medium.^[28]

The effect of this sequence of energy transfers (Figure 2d) is that the internal energy of the electron gas subsequent to photon energy absorption goes through: 1) a rapid and resonant enhancement (LSPR); 2) a confined electron gas redistribution (e–e) (athermic regime); 3) a fast decrease (e–ph scattering); and 4) a slow recovery of the initial state of equilibrium (ph–ph) (heat transfer to the surrounding medium).

To settle the theoretical background of thermoplasmonics and infer the main physical underlying rules that govern the temperature field generated by AuNPs, we start by taking into account that metals are not ideal conductors at optical frequencies; thus, the aforementioned e–ph collision represents the damping mechanisms for the LSPR phenomenon in AuNPs, which results in heat generation via the Joule mechanism. To calculate the temperature^[19a] in proximity to the AuNP surface, it is fundamental to determine the Joule effect's heat. Then, assuming a surrounding medium with no phase transitions and exploiting the determined physical quantities (heat power density), it is possible to solve the heat transfer equation and the general equations governing the heat distribution in the surrounding environment. We impose the balance of the energy: the total amount of thermal energy generated by a single AuNP must equal the amount of thermal energy generation (which accounts for the Joule effect), plus the thermal energy confined inside the AuNP. The actual ΔT experienced by AuNP depends on several parameters, namely its absorption cross-section σ_{abs} , its shape, the thermal conductivity k_m of the surrounding medium, the heat power Q , and the wavelength λ and irradiance I of the impinging light.^[29] More precisely, the temperature variation ΔT_{NP} of a uniformly charged AuNP surrounded by a homogeneous medium and possessing a thermal conductivity k_m is given by

$$\Delta T_{\text{NP}} = \frac{Q}{4\pi k_m R} = \frac{\sigma_{\text{abs}} I}{4\pi k_m r} \quad r > R \quad (3)$$

R and r are the NP radius and the distance from the center, respectively. The reverse proportionality between ΔT_{NP} and r highlights the NP's extraordinary capability to generate elevated thermal energy in the medium surrounding and proximity the NP (Figure 3a,b). The highest increment of temperature is generated at the NP surface (i.e., $r = R_{\text{NP}}$), and, because $\sigma_{\text{abs}} \propto V_{\text{NP}}$ (volume of the AuNP), it turns out to be proportional to the second power of the NP radius.^[30] The validity of Equation (3), is not restricted to spherical AuNPs only; indeed, a similar equation can be used also to extract surface temperatures of non-spherical AuNPs (e.g., Au nanorods, AuNRs) (Figure 3c,d), by including a dimensionless geometrical correction factor β in the denominator^[31]

$$\Delta T_{\text{nonspherical}} = \frac{\sigma_{\text{abs}} I}{\beta 4\pi k_m R_{\text{eff}}} \quad (4)$$

Where R_{eff} is the radius of a sphere having the same volume of the nonspherical AuNP; the factor β has been calculated for a large set of AuNPs morphologies with axial symmetry (i.e., rods, ellipsoids, discs) and its different values are reported elsewhere.^[32]

When a homogeneously distributed AuNP array is involved in a photo-induced heating process, several complex physical phenomena occur.^[33] To this purpose, Baffou et al.^[34] derived an analytical expression aimed at calculating the actual temperature increase at the center of a microscopic assembly of AuNPs, and an accurate theoretical model has been presented by Pezzi et al.^[35] In a system characterized by a considerable number (i.e., $\approx 10^{10}$) of homogeneously distributed AuNPs, every single AuNP can be seen as a star in the sky of the famous Olbers' paradox,^[35] so that also AuNPs close to the laser beam spot

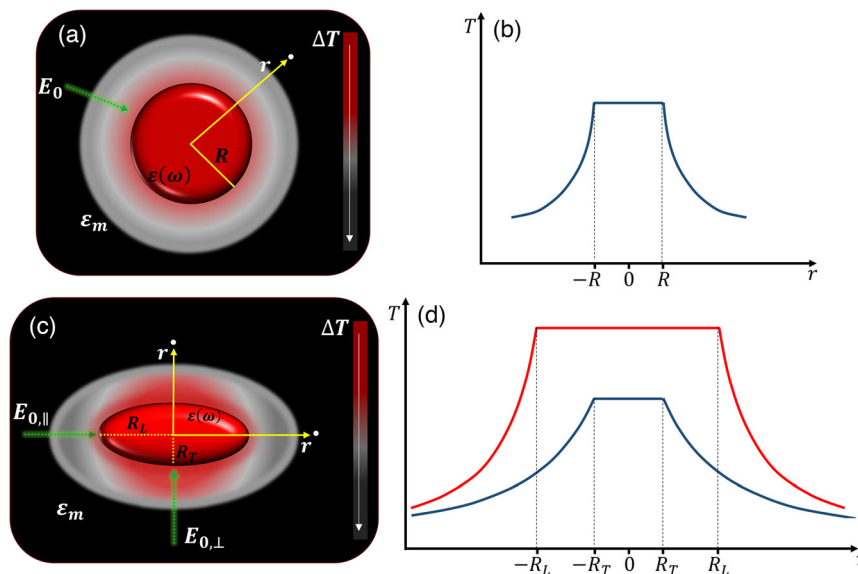


Figure 3. a) Sketch representing the conversion of light in thermal energy in AuNPs exhibiting spherical and c) elongated (AuNR) shapes along with their corresponding temperature profiles (b,d). The red curve (d) is obtained by irradiating the AuNR with light polarized along the longitudinal axis; the blue curve (d) is obtained irradiating the AuNR with light polarized along the transversal axis.

contribute to the bulk temperature variation, precisely like in Olber's paradox. The sky's global brightness is due to every single star's contribution. The elevated number and the homogeneous distribution of AuNPs allow for a macroscale continuum distribution, thus simplifying the equation for predicting the temperature increase. Therefore, assuming a bi-dimensional case where AuNPs are illuminated with a laser beam with a Gaussian profile, intensity I_0 , and radius w , the equation for ΔT is

$$\Delta T(r = 0) = 2\pi w \frac{V_{NP} \text{Im}(\chi_{NP})}{2\lambda k_H \sqrt{\epsilon_H}} \left| \frac{3\epsilon_H}{2\epsilon_H + \epsilon_{NP}} \right|^2 n_{NP} I_0 \quad (5)$$

where $\text{Im}(\chi_{NP})$ is the imaginary part of the electric susceptibility, k_H is the host medium thermal conductivity, ϵ_H , ϵ_{NP} are the surrounding medium and NP dielectric constant, and n_{NP} is the total NPs number.

From this expression, a lot of important information emerges: 1) the temperature variation ΔT , induced by a huge number of AuNPs, is proportional to the intensity of the laser: $\Delta T = \beta I_0$; 2) the angular coefficient β takes into account also the effective thermal conductivity k_H , which, depends on both the substrate and the surrounding medium; 3) ΔT can be increased by increasing both the spot size of the laser beam w or the number of irradiated AuNPs. The thermographic analysis evaluates temperature values on the entire area irradiated by the laser beam, empirically verifying the linear dependence of ΔT on the incident light intensity. This also leads to the simple derivation of the k_H value by using a trivial inverse relationship to deduce the angular coefficient of ΔT plotted as a function of I_0 . This theoretical model is valid: 1) for collective thermal effects produced by a huge number of NPs, and 2) for any NPs spatial distribution that does not allow geometrical simplification; in addition, 3) it can be easily extended to a 3D bulk distribution of AuNPs, thus further expanding its range of applicability.

4. Probing and Controlling Photothermal Heat Generation

Experimental research has been focused on determining the photothermal properties of AuNPs dispersed in several surrounding media, with the ability to measure the photo-induced temperature change. To this end, several techniques have been used such as the utilization of thermocouples,^[36] fluorescent materials,^[37] magnetic resonance imaging,^[38] scanning thermal imaging microscopy,^[39] and IR thermography.^[40] Each technique exhibits its strength and weakness. At the nanoscale, mechanical thermal probes, such as scanning thermal microscopy utilize a mechanical contact (tip) to detect the temperature change. Methodologies based on optical thermal probes are noninvasive and benefit from the possibility to combine them with the ubiquitous optical microscopy (Raman thermometry,^[41] photoacoustic thermometry^[42]). Of particular interest is the thermometry method based on the measurement of the fluorescence polarization anisotropy: by directly assessing the molecules' Brownian dynamics, it is possible to map the local temperature near nanometer-sized heat sources, with a 300 nm spatial resolution and a typical accuracy of 0.1 °C.^[43] Another compelling solution for nanoscale heating detection can be obtained by monitoring optical modifications

of the AuNPs surrounding matrix, exploiting some materials' thermoresponsive properties, like thermotropic cholesteric LCs.^[44] IR thermography is a noninvasive technique that provides a 2D temperature map with good spatial resolution and very high sensitivity (<0.05 °C) on a macroscale level.^[40b] In some cases, however, a macroscale average temperature measurement is not enough and may mask important information. Many fields would benefit from accurate and precise temperature measurements, such as electronics, integrated photonic devices, and biology. Furthermore, the state of most biosystems can be easily controlled by controlling heating at the single-cell level and, several photothermal-induced processes are at present under investigation: thermal-induced unfolding and denaturation of proteins,^[45] melting of DNA,^[46] phase transition of lipid membranes and vesicles,^[47] migration or fusion of living cells,^[48] and of course hyperthermia (temperature-induced cell death).^[49] The most substantial limitation to applying AuNPs to induce hyperthermia in the framework of cancer therapy comes from the fact that tumor ablation can be caused by increasing the local temperature above 42 °C. Indeed, the main goal of PPTT is to thermally eradicate the tumor tissue without causing damage to the surrounding healthy tissue; thus, there is a clear need of investigating local temperature variations of the illuminated area with high sensitivity (less than 0.5 °C).^[18] In addition, the analysis performed by using a thermal camera, despite its high sensitivity, is in fact limited in spatial resolution. An accurate, high-resolution, monitoring of temperature at the nanoscale could help understanding cellular behavior and optimizing externally induced processes, such as the PPTT-related ones. In the following paragraphs, we discuss macroscale investigations of bulk temperature via IR thermography. Subsequently, we exploit the possibility of employing temperature-sensitive materials for monitoring photo-induced temperature change. Specifically, LCs are the thermosensitive materials chosen to present our nanoscale thermometry technique. Their spectral characteristics (peak width and position) can be controlled by changing the physical system's temperature. Furthermore, to exploit the plasmonic heating generated by AuNPs in the framework of PPTT, a hydrogel was selected to work as the heat-responsive material; this choice enables to get closer to an environment as biocompatible as possible and to emulate the physiological cellular environment with a water-based skin-equivalent model.

4.1. IR Thermography

The collective properties and the photothermal efficiency of plasmonic NPs can be studied by performing bulk experiments.^[23] To qualitatively and quantitatively monitor the heating characteristics of a large ensemble of AuNPs nanoheaters dispersed in water or immobilized on rigid substrates, IR thermography can be efficiently used.

Although the human eye cannot perceive infrared (IR) radiation, the IR camera can detect it and convert it into a visual image representing thermal variations throughout or over a specific region of the sample.^[50] IR thermography has proved to be an accurate technique for precisely monitoring bulk temperature variations.^[51] It is a pretty versatile technique, which offers a plethora of possibilities. Thus, it is perfectly suitable for different applications in several research fields, such as automotive

applications^[52] and art conservation.^[53] IR imaging is based on the fact that any object at a temperature above absolute zero emits IR radiation, even if only weakly, due to the collisions between molecules within the material, a process that releases energy in the form of photons. The extraordinary ability to detect passive IR radiation makes thermal imaging cameras an indispensable tool in thermometry.^[54] It is, however, important to keep in mind that, in the thermographic-based analysis, the emittance of the object is a parameter that has to be taken into account (the emittance of a surface is defined as the ratio of radiation flux per unit area of a blackbody radiator's emitter at the same temperature and under the same conditions).^[55]

Figure 4a–c show some examples of IR images acquired with an IR thermal camera (FLIR A655sc), characterized by a very

high resolution of images of 640×480 pixels, thermal sensitivity $<0.03 \text{ }^\circ\text{C}$, and spatial resolution (IFOV) of $50 \text{ } \mu\text{m}$. A large number of pixels allow generating detailed and highly resolute images, from which it is easy to obtain the desired temperature information. In the IR images in Figure 4a–c a rainbow color palette (called “1234”) is used, in which the color gradient starts from yellow, for the hottest point, to dark blue, for the colder one; this provides a first evaluation, allowing to define the range and level of temperature. Later on, IR images are processed through a custom analysis software (the ResearchIR thermographic data acquisition and analysis software) that provides a wide variety of functions, from real-time image acquisition, to post-acquisition processing of thermographs (Figure 4d–g). A region of interest (ROI) can be selected in the image to carry out analysis of a

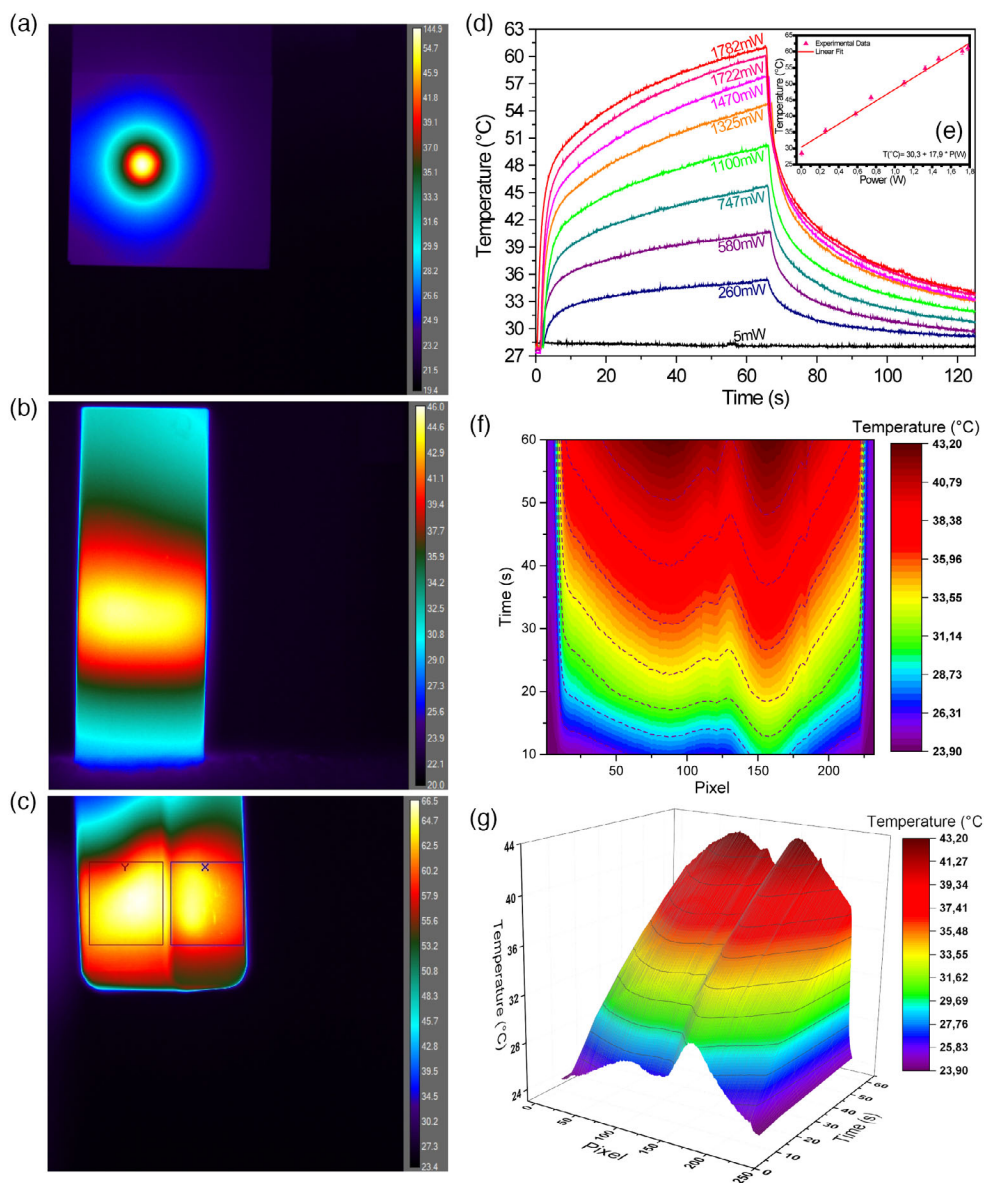


Figure 4. a) Representative IR thermographic images (color palette “1234”) extracted from experiments carried out with AuNRs deposited on a substrate and b,c) colloidal solutions of AuNPs contained in a quartz cuvette, along with d) illustrative graphs of the temporal behavior. e) Linear correlation between the maximum temperature and the power of the laser. f) 2D spatial map, and g) 3D spatial distribution of temperature.

single point, line profiles, averages of circle/rectangular areas, and 3D area.

Experiments were realized by photo-activating the AuNRs deposited on a glass substrate (Figure 4a) and dispersed in water (Figure 4b,c) with a CW laser source operating at 808 nm. The density of AuNRs deposited on the glass substrate is about $700 \text{ AuNR } \mu\text{m}^{-2}$ while the AuNRs aqueous solution has an optical density of 125, and it was diluted 1:35.

4.2. Liquid Crystal Thermometry

The characterization of the heat propagation from the photoheated AuNPs to the medium surrounding the same AuNPs is essential for realizing photothermal-based applications in different research fields such as nanomedicine, electronics, and optics. As such, photo-responsive and thermosensitive materials are crucial and represent a new avenue in nanotechnology. Simultaneously, the utilization of thermoplasmonics in optics allows realizing a novel generation of light-controlled optical components (Figure 5). This achievement has been enabled by combining light photoheated AuNPs and reconfigurable materials such as thermotropic cholesteric liquid crystals (CLCs), photocurable liquid crystal monomers, and nematic liquid crystals (NLCs).

Thermotropic CLCs are short pitch (P) chiral materials which organize in layers with no positional ordering of molecules within each layer, but exhibiting a mesoscopic order described by a helicoidal orientation of the director axis from layer to layer.

CLCs behave as 1D photonic bandgap systems where propagation of light of given wavelengths and polarization states is forbidden due to the helix periodicity.^[56] It is worth noting that the

spectral characteristics (width and position) of the photonic bandgap associated with the CLC helix can be controlled by applying an electric field, or changing the system temperature,^[57] or exposing the sample to suitable optical radiation.^[58]

In Figure 5a, b, we report on the possibility of combining AuNRs characteristics and CLC self-organization properties for simultaneously controlling the selective reflection of CLCs and the spectral position of the LSPR of AuNRs,^[44] both effects are obtained by exploiting the local heating induced by an external NIR light source. Compared to previously exploited techniques^[59] the reported method (see^[44] for more details) represents an innovative noninvasive tool. The properties of well-known materials such as CLCs are used for continuously monitoring photo-induced temperature variations around AuNRs, with high sensitivity. Figure 5b shows the CLC reflection band's behavior under illumination with a CW NIR pump beam ($\lambda_{\text{pump}} = 680 \text{ nm}$, $I_{\text{pump}} = 0.2 \text{ W cm}^{-2}$), for different illumination times. The CLC behaves as a mirror for all the colors (wavelengths) within the impinging white light's reflection band, which are back reflected. By photo-exciting the same area of the sample, the light-triggered activation of AuNRs produces heating with a consequent exchange with the surrounding medium (CLC in the actual case).^[60] Consequently, because of the photothermal heating, there is an elongation of the CLC pitch, followed by a linear red-shift of the reflection band. In Figure 5b, it is noticeable that while increasing the exposure time (for a fixed pump intensity), there is a progressive attenuation and a redshift (more than 130 nm) of the reflection band associated with the gradual increase of the average temperature of the illuminated area. In fact, according to Equation (6)

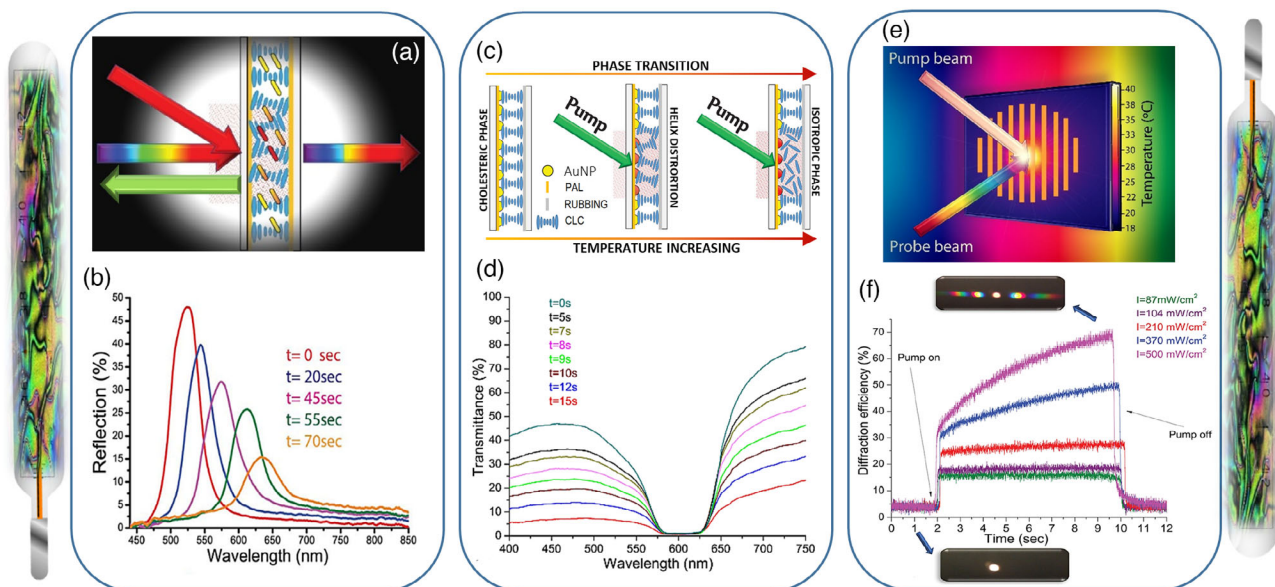


Figure 5. a) Sketch of the AuNRs/CLCs sample upon laser beam illumination and b) sample's reflection spectra acquired at different illumination times. c) Drawing of the AuNPs/CLCs sample in which the green arrow represents the pump beam (off, left; on middle and right). d) The sample's transmission spectrum was acquired with probe white light circularly polarized as a function of the illumination time. e) Sketch of a reverse-mode diffraction grating made of AuNRs, NLC, and PLC. f) First-order diffraction efficiency as a function of the intensity of the pump laser along with the corresponding diffraction patterns (pump off, lower image; pump on, upper image). The two thermometers that enclose the figure recall the paragraph's title: liquid crystal thermometry. Adapted with permission.^[65] Copyright 2019, American Chemical Society. Adapted with permission.^[44] Copyright 2013, John Wiley and Sons. Adapted with permission.^[62] Copyright 2018, Springer Nature.

$$\lambda_0 = \langle n \rangle P \quad \langle n \rangle = \frac{n_e + n_o}{2} \quad (6)$$

$$\Delta\lambda = \Delta n P = (n_e - n_o)P \quad (7)$$

The reflection band's position depends on the pitch P , which varies (increases) with temperature. Consequently, if the temperature increases, there is a reduction of the number of periods in the sample that produces an attenuation and a broadening (Equation (7)) of the reflection band.^[61]

The second application deals with realizing a thermoresponsive plasmonic architecture (1 in.²) of randomly distributed spherical AuNPs stuck on a rigid substrate and layered with a CLC that works as an active surrounding medium for simultaneously controlling both photonic and plasmonic properties of this hybrid system.^[62] A photothermal heating effect due to the LSPR mechanism is generated by pumping the AuNPs array with a resonant light beam ($\lambda_{\text{pump}} = 532$ nm, high absorption range of spherical AuNPs).

The generation of light-triggered heating produces a phase change of the CLC film (from cholesteric to isotropic) with a consequent modulation of the LSPR frequency (plasmonic effect) and selective reflection (photonic effect). The interplay between photonics and plasmonics allows detecting plasmonic heating via LCs thermometry. By increasing the illumination time (from 0 to 15 s, $I_{\text{pump}} = 60$ mW cm⁻²) (Figure 5d), the AuNPs generate a Joule heating that dissipates in the sample (CLC film) with consequent distortion of the CLC organization (Figure 5c, middle image) that makes an attenuation ($\approx 80\%$) and broadening (≈ 5 nm) of the photonic bandgap (Figure 5d). The attenuation of the photonic bandgap (Figure 5d) is attributed to the increasing of the scattered/transmitted light, whereas its broadening is due to a modest chirping of the CLC pitch profile generated by the temperature gradient through the sample (hot to cold). By further increasing the illumination time (from 15 to 19 s), the CLC film undergoes a complete phase transition (from 15 to 19 s), and the sample becomes optically clear (isotropic phase). Consequently, the reflection band is totally suppressed (Figure 5c, right image). Curves reported in Figure 5d have been acquired by utilizing a right circularly polarized light to remove the AuNPs absorption band's effect. A completed characterization of the samples' spectral response for polarized and unpolarized white light sources and the details about the dynamic of the sample are reported in Ref. [62]. It is important mentioning that in both experiments reported in Figure 5a,c, the photonic and plasmonic properties are very well separated. In this condition, the structural effect of the CLC cannot affect the AuNRs or the AuNPs by means of photonic-band edge, as reported in Kim's study^[63] and Ricci's study.^[64] In a different approach, we used the thermoplasmonic heating of AuNRs to activate and deactivate the diffractive properties of a reverse-mode diffraction grating (Figure 5e) made of NLC and a polymerizable liquid crystal (PLC).^[65,66] The grating is completely "hidden" and appears as a transparent optical window in the off state because of the initial refractive-index match between the PLC-rich and NLC-rich regions. Figure 5f shows the temporal behavior of the first-order diffraction efficiency acquired for different values of the pump laser's intensity (from 87 to 500 mW cm⁻²) while the probe laser intensity is kept constant. Photo-exciting the AuNR-containing

structure with a resonant laser beam ($\lambda = 808$ nm) causes thermoplasmonic heating, there is a change in the refractive index between the PLC and NLC, which results in the formation of a highly efficient diffractive structure. In addition, we showed^[65] that the same structure can be used to realize a variable waveplate, thus learning an innovative methodology for measuring the photo-induced temperature changes and controlling a laser source's polarization state. This new class of optical components does not require optical power in the diffraction-off state, thanks to the reverse-mode working principle. Our results clearly demonstrate that thermoplasmonics with AuNPs is a new opportunity in the realization of reconfigurable optical components. This enormous opportunity opens a new scenario in light-controlled photonics that could prove particularly useful when using polymers that do not allow an electric-field control. What's more, NPs with exotic shapes such as triangles, cubes, and hexagons could help develop useful in developing on-chip photothermal sensors, thus adding a new level of flexibility to existing photonic devices. We are pushing this versatility even further by realizing a new generation of biomedical thermal sensors by exploiting the interplay between thermoplasmonics and water-based liquid crystal thermometry.

4.3. Thermosensitive Hydrogel: PNIPAm for Photonic Applications

In recent years, temperature-responsive hydrogels have been extensively used for numerous bio-based applications and are now widely used as biomaterials. They are biocompatible because their physicochemical properties are similar to those of the living tissues, for example, they are characterized by high water content, soft and rubbery consistency, and low interfacial tension with water or biological fluids. Among them, poly(*N*-isopropylacrylamide) (PNIPAm) and its derivatives like poly(*N*-isopropylacrylamide-*co*-*N*-isopropylmethacrylamide) P(NIPAm-*co*-NIPMAM) are water-soluble, temperature-responsive, materials that undergo reversible phase transitions (coil-to-globule-type transition)^[67] at a specific temperature.^[68] PNIPAm is a material promising for bio-related experiments^[69] for its ability to become hydrophilic from hydrophobic for temperatures above 37 °C.^[70] Combining the strengths of hydrogel and AuNPs, with unique stimuli responsivity, PNIPAm microgels have found numerous biomedical applications, such as biosensing and PPTT.^[71] PNIPAm embedding AuNRs has been synthesized^[72] to develop theranostic nanoplat-forms with photothermal and thermoresponsive properties for novel tumor-targeting techniques. Poly(*N*-isopropylacrylamide), like P(NIPAm-*co*-NIPMAM), possesses excellent mechanical, thermal, and chemical stability, which enables it to exhibit a very long shelf life.^[73] For these reasons, P(NIPAm-*co*-NIPMAM) has been utilized in several fields such as optics,^[74] solar energy,^[75] electronics,^[76] catalysis,^[77] and sensing.^[78] The unique combination of Au nanostructures' optical properties and the smart behavior of a thermosensitive polymer in the form of Au-hydrogel has attracted great interest.^[79] In this section, an investigation of innovative optical attenuators made of AuNRs dispersed in crystal-clear P(NIPAm-*co*-NIPMAM) films is reported.^[80] The polymeric film, changing from the hydrophilic to the hydrophobic state due to AuNRs nanoheaters, undergoes a release of water, which produces

an attenuation of its optical transparency that can be remotely controlled thanks to the photothermal properties of AuNRs. The phenomenon enables developing a light-controllable optical attenuator and the possibility to control and detect photo-induced heat from the dispersed AuNRs.

To realize high-quality *P(NIPAm-co-NIPMAm)/AuNRs* samples, the surface of Petri dishes (WillCo-dish, GWSt-5030) with 30 mm diameter was subject (15 min) to an oxidation plasma (by Diener Electronic GmbH-Co. KG, Zepto) treatment (Figure 6a). The solution (*P(NIPAm-co-NIPMAm)/AuNRs*) was deoxygenated for 10 min using an Argon blowing setup. After that, a small amount (0.5 mL) of the solution was poured into each Petri dish (Figure 6b). The immersion of the samples into an ice bath before the top irradiation procedure (Figure 6c) allows to keep the temperature below 20 °C during the photo-polymerization process (1 min, UV light, source by Dymax Europe GmbH, 5000-PC). The *P(NIPAm-co-NIPMAm)/AuNRs* discs were removed (Figure 6d) from the Petri dishes and stored in water at room temperature. Figure 6e highlights the sample's excellent optical transparency.

Light-triggered experiments were carried out using the thermographic optical setup illustrated in Figure 7. It makes use of a CW pump laser ($\lambda = 808$ nm) and a thermal camera for

triggering and monitoring the photothermal properties of AuNRs. In contrast, the spectral properties are monitored using a compact UV-vis spectrophotometer. All the other technical and experimental details are reported in Ref. [80].

By keeping OFF the pump beam (Figure 8a), the *P(NIPAm-co-NIPMAm)* sample maintains its natural optical transparency, and the probe (white) light is transmitted. In contrast, by turning ON the pump beam ($I = 5060$ mW cm⁻²), the photothermal-induced phase transition produces an apparent attenuation of the probe (white) light (Figure 8b). The sample's photothermal-activated area is evident in Figure 8c,d, where the probe beam is turned OFF. To test the stability of the samples after storing them in water, a detailed characterization of their morphological and optical properties was performed. Four identical samples were fully immersed in distilled water and investigated at $t = 0$ days, $t = 1$ day, $t = 30$ days, $t = 45$ days by: 1) field emission scanning electron microscope (FE-SEM); 2) pump-probe optical setup. Moreover, samples were inspected by TEM to check if the light-induced thermal heating produces any kind of detectable change (e.g., reshaping) of AuNRs.

Figure 9a–d clearly show that the prolonged immersion in water does not produce any change in the samples' morphology. Indeed, no presence of structural defects is visible at this level

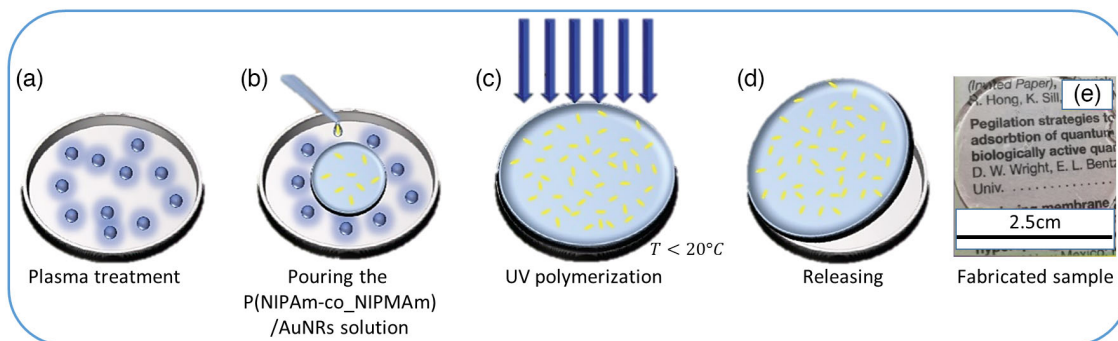


Figure 6. Schematic of the preparation process of the *P(NIPAm-co-NIPMAm)/AuNRs* sample.

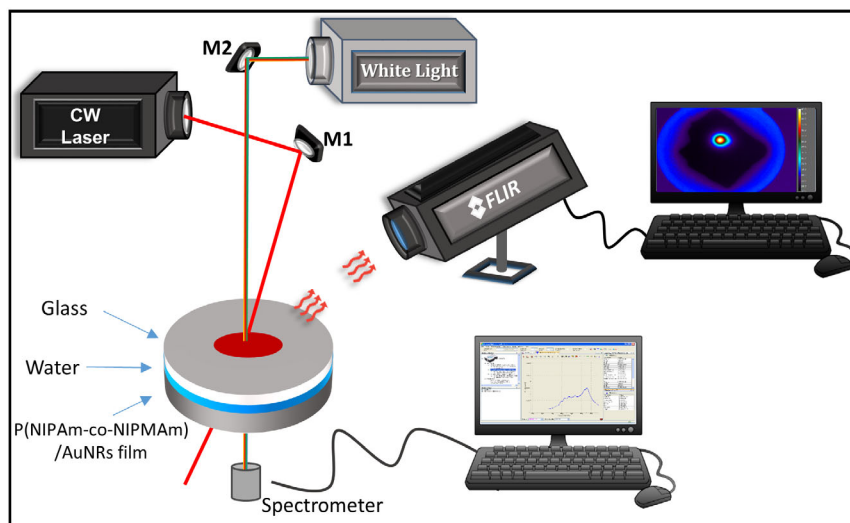


Figure 7. Thermo-optical setup for sample characterization.

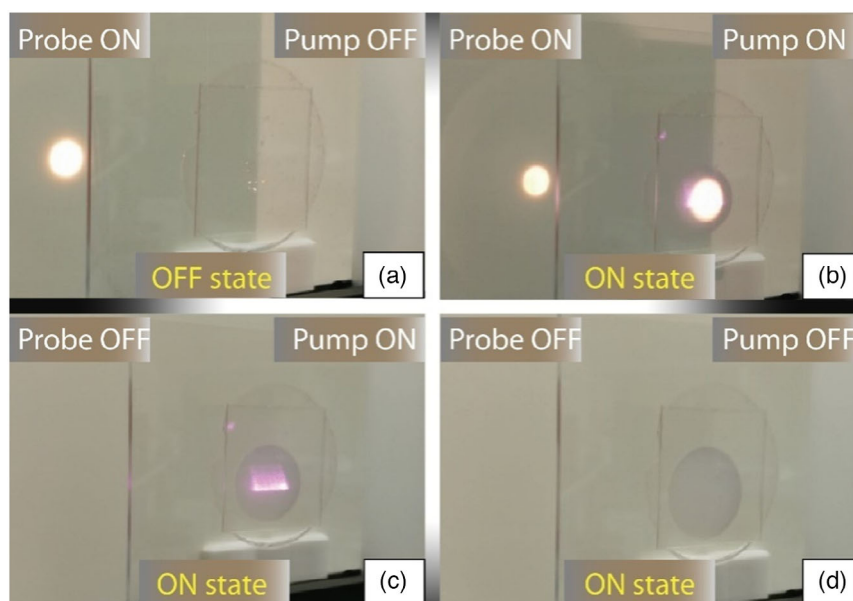


Figure 8. Photographs of the sample in different operational states for different combinations of the pump-probe beams: a) OFF and (b–d) ON. Reproduced with permission.^[80] Copyright 2020, John Wiley and Sons.

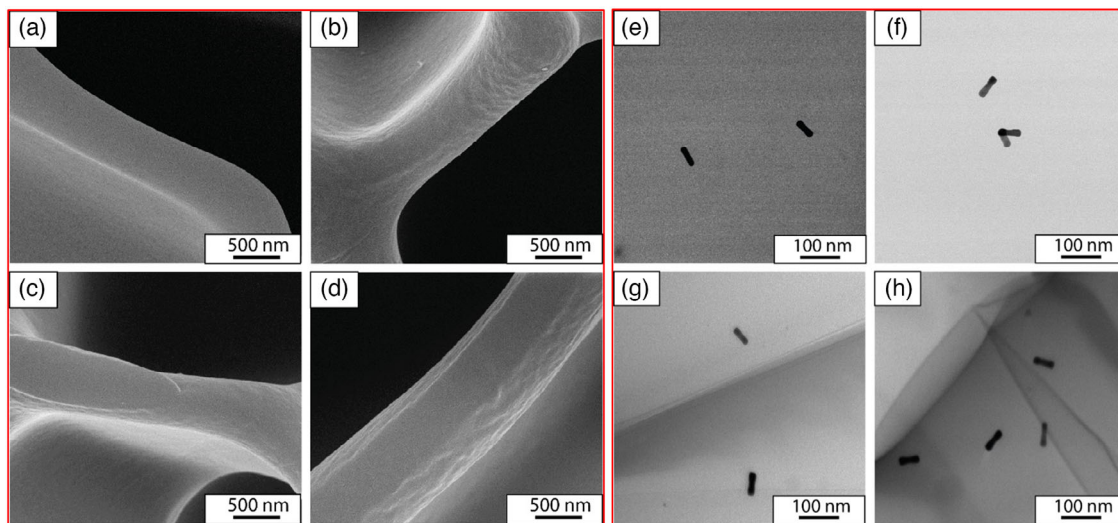


Figure 9. a) FE-SEM analysis of samples at different hydration times: $t = 0$ days, b) $t = 1$ day, c) $t = 30$ days, d) $t = 45$ days. TEM analysis of the samples after different cycles of photo-switching experiments: e) 0 cycles; f) 1 cycle; g) 5 cycles; h) 10 cycles. Adapted with permission.^[80] Copyright 2020, John Wiley and Sons.

of magnification, highlighting the extraordinary capability of the samples to retain their morphological properties even after 45 days of continuous hydration. Figure 9e–h, confirm that even after cycling the samples up to ten times (Figure 9h), the shape of AuNRs turns out to be very similar to the one observed before starting the photo-switching experiments (Figure 9e). This is clear evidence that AuNRs are stable under resonant light beam illumination, and no reshaping processes of AuNRs take place.

Photo-switching experiments (by cycling the sample up to 10 times) at each hydration time were carried out by using the optical setup shown in Figure 7. Figure 10 reports the excellent

reversibility of the transmitted intensity: no relevant changes in the response times and optical contrast are observed. To exploit the possibility of improving the sample's performance, we realized a thermo-optical light attenuator with improved response times by increasing the concentration of AuNRs. Picture of a sample PNIPAm + 40 wt% of AuNRs, $C_{\text{AuNRs}} = [3 \times 10^{-9} \text{ M}]$ is shown in Figure 11a. Comparing the previously reported optical attenuator (Figure 6e), it is evident that the increase in the AuNRs amount has induced a substantial color change (pinkish tint). In the spectroscopic response shown in Figure 11b, a shift of the LSPR peak, of about 38 nm, can be observed, which is due to

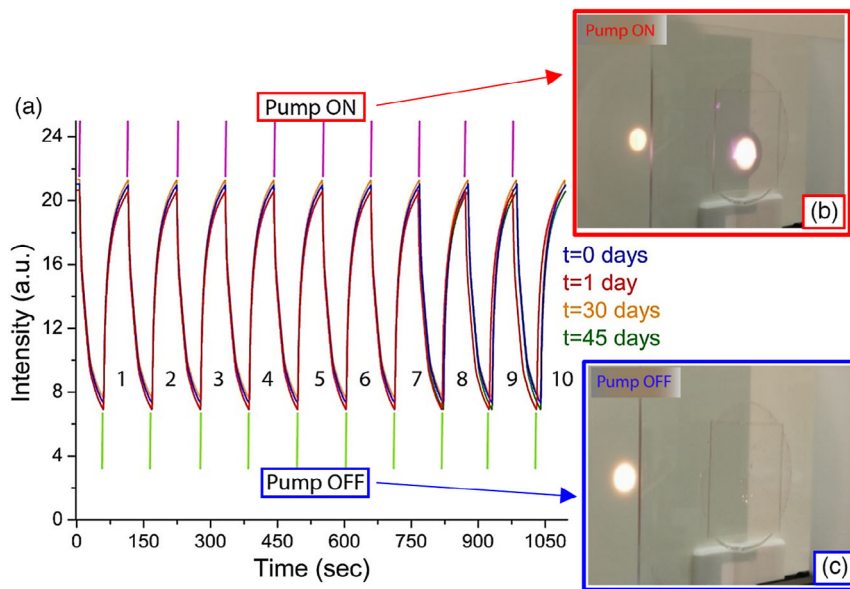


Figure 10. Reversible changes of the transmitted intensity of samples induced by cycling (from 0 to 10) the pump beam ON and OFF. Samples were tested at different storage times in water (from 0 to 45 days). Adapted with permission.^[80] Copyright 2020, John Wiley and Sons.

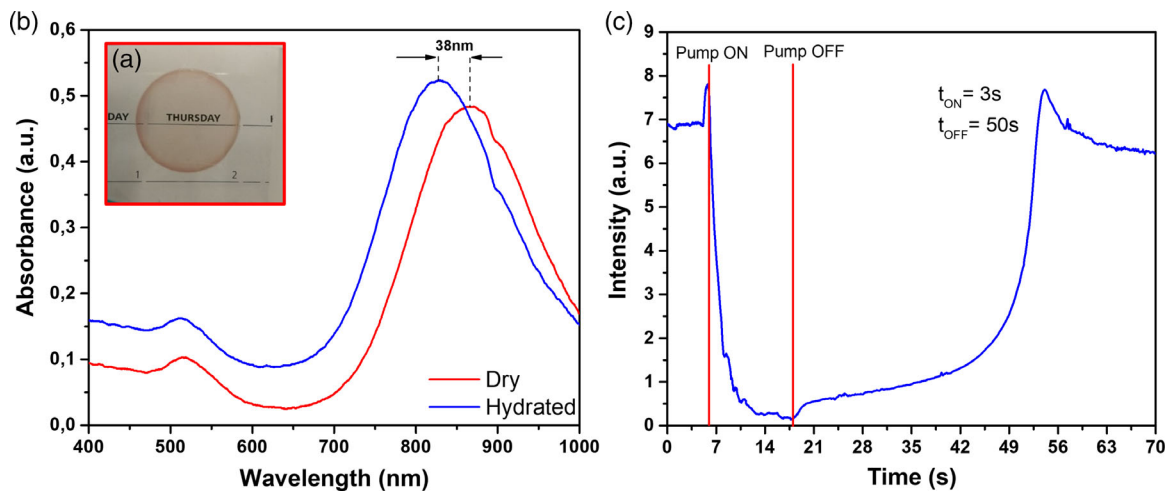


Figure 11. a) Picture of the sample PNIPAm + 40 wt% of AuNRs, $C_{\text{AuNRs}} = [3 \times 10^{-9} \text{ M}]$. b) Spectral response of the sample. c) Reversible change of the transmitted intensity.

the transition from dry to hydrated state of the sample. Overall, the device with an increased concentration of AuNRs (40 wt%) inside the polymer film is more performing with an improved t_{on} (activation) and t_{off} (deactivation) response times (Figure 11c). Response times of the sample reported in Figure 10 are 52 and 55 s, respectively, achieved using a laser intensity $I = 5060 \text{ mW cm}^{-2}$. In contrast, with the improved sample (Figure 11a), the intensity needed to trigger the transparent/opaque conversion was reduced to $I = 1060 \text{ mW cm}^{-2}$ while providing better response times (3 and 50 s, respectively).

The proposed light attenuator exhibits excellent optical and mechanical properties and works without electricity. These results open a new opportunity in energy-saving optical devices and can be utilized to promote green photonic applications.

5. Thermosensitive Hydrogel for Biomedical Applications

Light-responsive bioinspired materials constitute a new, breakthrough biomedical treatment thanks to the possibility to use NIR-light. With the assistance of plasmonic hydrogels, nanostructured materials make it possible to manipulate light at the nanoscale.

A few research teams have investigated the possibility of developing smart plasmonic hydrogels for biomedical applications focusing their scientific activities on the use of different kind of polymer matrices, including chitosan-based hydrogels,^[81] polyvinyl alcohol (PVA),^[82] DNA hydrogel,^[83] and poly-(ethylene glycol) diacrylate (PEGDA).^[84] Although a broad range of

hydrogels could be applied in this field incorporating AuNPs in their polymer networks, thermoresponsive polymers (e.g., PNIPAM) stand out from the crowd since, in this case, light could trigger a cascade-like series of responses and new functionalities.

Recently, we developed a biomimetic nanoplatform with a nature-inspired hierarchical architecture based on a combination of plasmonic NPs P(NIPAm-co-NIPMAm) hydrogel and electrospun nanofibers (Figure 12a).^[85] The mesoglea structure of jellyfishes has inspired the hierarchical structure of the developed nanoplatform (Figure 12b). The inspiration from mesoglea is based on two similarities with our system. The first is the structural affinities that include layered porous nanofibrous structure combined with hydrogel, while the second is the functional analogy related to high water expulsion during the hydrogel contraction that takes place upon irradiation by NIR light. This multifunctional nanostructured platform can efficiently convert light to heat, promoting a cascade of structural changes capable of inducing the on-demand release of drugs previously loaded into the electrospun fiber matrix (Figure 12c). The stable biomaterial composed of a plasmonic hydrogel anchored to polymer-based nanofibers (Figure 12d) showed outstanding biocompatibility and unique light-activated functionalities, paving the way for the development of nanostructured devices for combined chemo- and photothermal therapy using a novel polytherapeutic treatment approach. The nanoplatform applicability was proved by subjecting skin cells and pig tissues to the suggested treatment. The developed multifunctional biomaterial allows drugs to be delivered simultaneously with PPTT using the synergic action of multitherapy for more efficiency in cancer and antibacterial

treatments. This novel approach will help to overcome the main limitation of conventional drug delivery systems, thanks to the possibility to trigger the release of bioactive molecules on-demand by light irradiation.

Although conventional polymers cannot produce a cascade response to light stimulations, a few types of these hydrogels have been studied to fabricate NIR-responsive biomaterials due to their potential application in translational medicine. A simple method for fabricating injectable and NIR-responsive chitosan and alginate hydrogels has been developed by Zeng et al.^[86] First, AuNPs with a proper aspect ratio were synthesized through a seed-mediated growth method. Dopamine-modified alginate (Alg-DA) has been used to modify AuNPs with a mussel-mimic design, and finally, AuNP-doped chitosan/dopamine-modified alginate composite hydrogel (CGP/Alg-DA/AuNRs) were prepared. The nanostructured composite showed strong absorption in the NIR region and the ability to translate the energy to heat, exhibiting excellent photothermal conversion efficiency. Moreover, *in vivo* antitumor efficiency of the CGP/Alg-DA/AuNR hydrogels with PPTT was also investigated by injecting the nanomaterials into xenograft HepG2 tumor models. These tests proved that the smart hydrogel could strongly reduce tumor growth without any other side effects under PPTT. Even if the tumor was not killed *in vivo*, the hydrogel already showed an outstanding PPTT efficacy in the absence of antitumor molecules. The use of CGP/Alg-DA/AuNR hydrogels for anticancer therapy is still in the early stages; therefore, the material needs to be optimized encapsulating specific anti-tumor drugs to improve its effectiveness in the treatment of tumors.

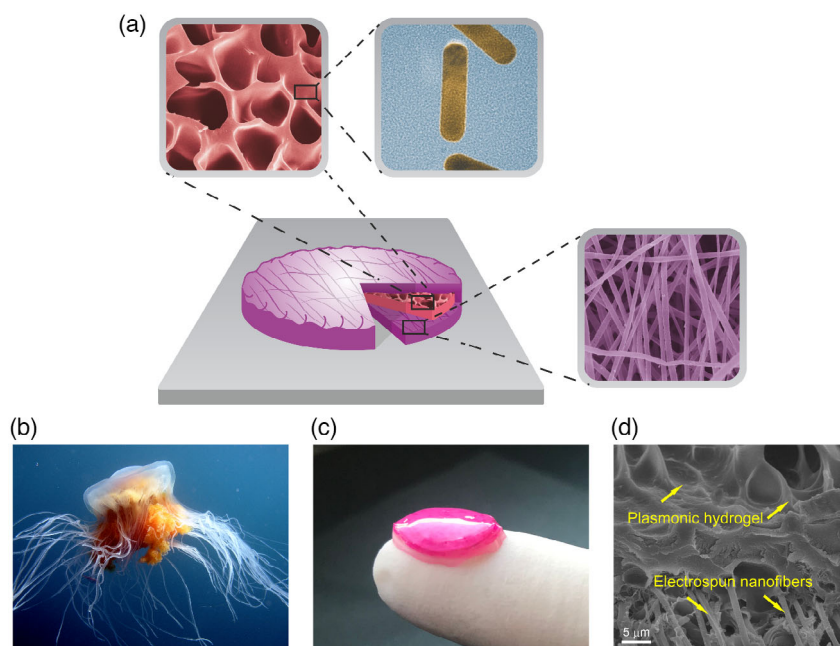


Figure 12. a) Sketch showing the developed platform structure: a P(NIPAAm-co-PNIPMAAm) hydrogel layer embedding AuNRs is encapsulated between two electrospun nanofiber mats loaded with a drug model. b) Photograph of a Phacellophora Camtschatica jellyfish. c) Photograph of a nanostructured pillow loaded with rhodamine B. d) Cross-section of the fiber-hydrogel interface in the smart biomaterial's inner structure shows the anchorage between the hydrogel and the nanofibrous layer. Reproduced with permission.^[85] Copyright 2020, American Chemical Society.

Lin et al. proposed the synthesis of a multifunctional gelatin methacrylate (GelMA) filled with Au nanobipyramids (Au NBPs) having the ability to release an antibiotic drug and PPTT features under NIR irradiation for the treatment of periodontal disease.^[87] A modified Stober method was applied to cover previously synthesized Au NBPs with mesoporous silica to obtain mesoporous silica-coated Au NBPs (Au NBPs@SiO₂). The hybrid nanoparticles were used as nanofillers to synthesize disk-shaped GelMA-Au NBPs@SiO₂ hydrogels incorporating minocycline (MINO) as a bioactive drug. When the nanostructured hydrogel was irradiated by NIR light, Au NBPs@SiO₂-embedded hydrogel absorbs photons and converts them into heat. This process provoked a slight reduction in volume, which favored the bioactive molecules' release using a similar but less effective mechanism than P(NIPAm-co-NIPMAm). In addition, the smart hydrogel possesses 90% and 66.7% antibacterial efficacy against *Porphyromonas Gingivalis* by antibiotic and photothermal treatment, respectively. Concluding, the controlled drug delivery and physical sterilization synergetic effects of the Au NBPs@SiO₂-embedded hydrogel make it a promising material for the high-efficacy treatment of periodontal disease.

6. Thermoplasmonics in the Fight Against COVID-19

In the fight against COVID-19, an emergency that has hit the entire world population in a completely unpredictable and irrepressible way, turning into a real pandemic, there are also and

above all the solutions offered by smart nanotechnologies. The need to realize a new generation of smart face masks with high filtration levels and self-sterilization properties is mandatory, especially for healthcare professionals. UV and thermal disinfection are among the oldest and simplest disinfection methods, relying on light or heat utilization to kill bacteria or viruses. UV and thermal disinfection are commonly used to sterilize medical apparatus. The heat or the UV radiation delivered to treated surfaces by uniform heating or UV lamps, besides being chemical-free, are strongly germicidal. Thus, they are routinely used to disinfect critical medical equipment. However, the uniform UV or thermal disinfection's main drawbacks are the impossibility to confine the light/heating in the desired region and the time-consuming method because of the slow UV/heat penetration rate. The extraordinary properties of AuNPs to convert suitable radiation into thermal energy (photothermal effect) have marked their application in high precision cancer treatment through the so-called PPTT. In particular, AuNPs-mediated thermoplasmonics offer many opportunities, starting from diagnosis and screening using ultra-sensitive biosensors^[10] to detect dangerous pathogens, the defense against these agents through the implementation of smart masks,^[88] and the eradication of pathogens through photo-induced heat. Getting inspired by this opportunity, the photothermal properties of AuNRs have been utilized for localizing and improving the heat generation and penetration, thus opening a new avenue for realizing a reusable and on-demand disinfected facemask.

Figure 13a shows an FFP2 respirator with the addition of AuNRs water dispersion. The thermographic analysis

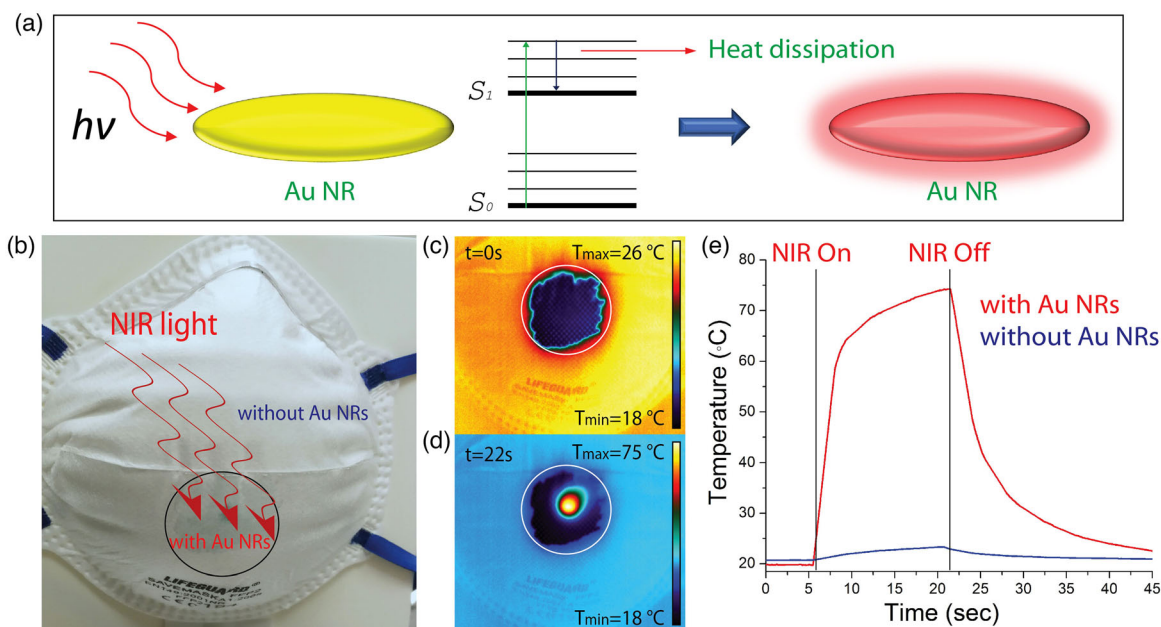


Figure 13. a) Schematic of the photothermal conversion process of AuNRs upon light irradiation. b) Photothermal responsive FFP2 (N95) respirator containing a drop-casted Au NRs dispersion (black circle) along with a thermographic view of the same region exposed to NIR laser ($\lambda = 810 \text{ nm}$; $I = 200 \text{ mW cm}^{-2}$) acquired at c) $t = 0 \text{ s}$, and d) $t = 22 \text{ s}$. e) Temperature profiles of the pristine (blue curve) and Au NRs treated respirator by turning ON and OFF the NIR laser beam. Water dispersed Au NRs ($C = 3.2 \times 10^{-9} \text{ M}$) have longitudinal and transversal LSPR bands centered at 775 and 524 nm, respectively. The dynamic IR thermographic analysis was carried out using a FLIR (A655sc) thermal camera that produces thermal images of 640×480 pixels with an accuracy of $\pm 2 \text{ }^\circ\text{C}$. The thermal camera was suitably equipped with a close-up IR lens characterized by a magnifying factor of 2.9 \times , a spatial resolution (IFOV) of 50 μm , and a reduced working distance. Reproduced with permission.^[88] Copyright 2021, John Wiley and Sons.

(Figure 13c,d) reporting the ON/OFF laser beam situations shows the efficient light-to-heat NIR light conversion mediated by the AuNRs, which leads to a maximum temperature of 75 °C in a short time interval. The thermal curve further supports this result as a function of time (Figure 13e, red curve) obtained by selecting a circular ROI on the sample. The control experiment (Figure 13e, blue curve) performed on the pristine area of the FFP2 did not show any significant temperature increment, thus confirming the outstanding photothermal properties of AuNRs, as schematized in Figure 13a. Under the outbreak background of COVID-19, this proposed face mask with smart nano-assisted destruction of pathogens can provide a reliable and easy-to-implement prevention tool to contain the pandemic spread.

7. Conclusion

A new light in optics and bio-photonics is offered by utilizing and applying the thermo-optical properties of AuNPs. Under suitable light illumination, AuNPs behave as nanosource of heating, opening a new scenario to realize all-optical components and biomedical applications. This compelling opportunity has been achieved by bridging “hot” AuNPs and temperature-sensitive materials, such as liquid crystals (LCs) and hydrogels. In this perspective, we have reported a new generation of light-triggered optical components, working as tunable mirrors, optical attenuators, switchable diffraction gratings, and smart windows. They are all based on the possibility of monitoring and exploiting the AuNPs’ photothermal properties thanks to the thermo-responsivity of temperature-sensitive materials. The proposed devices can be easily integrated into conventional heaters or regular thermometers for realizing a new generation of optoelectronic devices with high accuracy and visual detection of the monitored temperature.^[6,8] We have also highlighted the possibility of realizing a new generation of biomedical applications by exploiting the photothermal heating of AuNPs. Ranging from light controlled drug-release to the ongoing battle against COVID-19, thermoplasmonic-based AuNPs represents a new weapon for realizing a new generation of medical devices. These new concepts can be easily extended to other photonic and biomedical applications, making a paradigm shift in modern optics and bio-photonics thanks to the possibility of realizing light controlled innovative devices based on a thermoplasmonic mechanism.

Acknowledgements

This work was supported by funds received from Air Force Office of Scientific Research (AFOSR), Air Force Research Laboratory (AFRL) and USA. Air Force grant number FA9550-18-1-0038 (P.I.L. De Sio, EOARD 2017-2020), and the Materials and Manufacturing Directorate, AFRL; by the National Agency for Academic Exchange (NAWA) grant no. PPI/APM/2018/1/00045/U/001 and the First TEAM grant number POIR.04.04.00-00-5ED7/18-00, conducted within the framework of the First TEAM program of the Foundation for Polish Science (FNP), and cofinanced by the European Union under the European Regional Development Fund. The article was written through the contributions of all authors. All authors have approved the final version of the manuscript.

Conflict of Interest

The authors declare no conflict of interest.

Keywords

active plasmonics, liquid crystals, nanomaterials, optics, plasmonics, polymers

Received: December 19, 2020

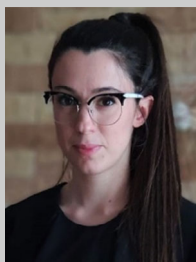
Revised: March 18, 2021

Published online: June 25, 2021

- [1] a) G. Baffou, F. Cichos, R. Quidant, *Nat. Mater.* **2020**, 1; b) H. Park, D.-J. Lim, J. B. Vines, J.-H. Yoon, N.-E. Ryu, *Front. Chem.* **2019**, 7, 167.
- [2] S. A. Maier, *Plasmonics: Fundamentals and Applications* (Ed: S. A. Maier), Springer Science & Business Media, New York, NY **2007**, pp. 65–88.
- [3] G. Baffou, R. Quidant, C. Girard, *Appl. Phys. Lett.* **2009**, 94, 153109.
- [4] M. I. Stockman, K. Kneipp, S. I. Bozhevolnyi, S. Saha, A. Dutta, J. Ndukaife, N. Kinsey, H. Reddy, U. Guler, V. M. Shalaev, *J. Optics* **2018**, 20, 043001.
- [5] L. R. Hirsch, R. J. Stafford, J. A. Bankson, S. R. Sershen, B. Rivera, R. Price, J. D. Hazle, N. J. Halas, J. L. West, *Proc. Natl. Acad. Sci.* **2003**, 100, 13549.
- [6] a) M. R. Ali, Y. Wu, M. A. El-Sayed, *J. Phys. Chem. C* **2019**, 123, 15375; b) M. R. Ali, I. M. Ibrahim, H. R. Ali, S. A. Selim, M. A. El-Sayed, *Int. J. Nanomed.* **2016**, 11, 4849; c) A. Kharlamov, A. Tyurnina, V. Veselova, O. Novoselova, A. Filatova, O. Kovtun, *J. Nanomed. Nanotechnol.* **2013**, 4, 2.
- [7] a) N. S. Abadeer, C. J. Murphy, *J. Phys. Chem. C* **2016**, 120, 4691; b) X. Huang, M. A. El-Sayed, *Alexandria J. Med.* **2011**, 47, 1; c) C. Ayala-Orozco, C. Urban, S. Bishnoi, A. Urban, H. Charron, T. Mitchell, M. Shea, S. Nanda, R. Schiff, N. Halas, *J. Control. Release* **2014**, 191, 90; d) J. R. Cole, N. A. Mirin, M. W. Knight, G. P. Goodrich, N. J. Halas, *J. Phys. Chem. C* **2009**, 113, 12090; e) E. B. Dickerson, E. C. Dreaden, X. Huang, I. H. El-Sayed, H. Chu, S. Pushpanketh, J. F. McDonald, M. A. El-Sayed, *Cancer Lett.* **2008**, 269, 57.
- [8] a) G. Han, P. Ghosh, M. De, V. M. Rotello, *NanoBiotechnol.* **2007**, 3, 40; b) F. Annesi, A. Pane, M. A. Losso, A. Guglielmelli, F. Lucente, F. Petronella, T. Placido, R. Comparelli, M. G. Guzzo, M. L. Curri, R. Bartolino, L. De Sio, *Materials* **2019**, 12, 1530.
- [9] A. Kumar, B. Mazinder Boruah, X.-J. Liang, *Journal of Nanomater.* **2011**, 2011.
- [10] a) G. Qiu, Z. Gai, Y. Tao, J. Schmitt, G. A. Kullak-Ublick, J. Wang, *ACS Nano* **2020**, 14, 5268; b) R. Samson, G. R. Navale, M. S. Dharne, *3 Biotech* **2020**, 10, 1.
- [11] S. Talebian, G. G. Wallace, A. Schroeder, F. Stellacci, J. Conde, *Nat. Nanotechnol.* **2020**, 15, 618.
- [12] O. Neumann, A. S. Urban, J. Day, S. Lal, P. Nordlander, N. J. Halas, *ACS Nano* **2013**, 7, 42.
- [13] S. V. Boriskina, M. A. Green, K. Catchpole, E. Yablonovitch, M. C. Beard, Y. Okada, S. Lany, T. Gershon, A. Zakutayev, M. H. Tahersima, *J. Opt.* **2016**, 18, 073004.
- [14] G. L. Liu, J. Kim, Y. Lu, L. P. Lee, *Nat. Mater.* **2006**, 5, 27.
- [15] X. Zhu, C. Vannahme, E. Højlund-Nielsen, N. A. Mortensen, A. Kristensen, *Nat. Nanotechnol.* **2016**, 11, 325.
- [16] J. C. Ndukaife, A. V. Kildishev, A. G. A. Nnanna, V. M. Shalaev, S. T. Wereley, A. Boltasseva, *Nat. Nanotechnol.* **2016**, 11, 53.

- [17] a) S. Wang, K. Komvopoulos, *J. Appl. Phys.* **2018**, *124*, 185109; b) G. Baffou, R. Quidant, in *World Scientific Handbook of Metamaterials and Plasmonics*, World Scientific Publishing, Singapore p. 379.
- [18] L. De Sio, T. Placido, R. Comparelli, M. L. Curri, M. Striccoli, N. Tabiryan, T. J. Bunning, *Prog. Quantum Electron.* **2015**, *41*, 23.
- [19] a) A. O. Govorov, W. Zhang, T. Skeini, H. Richardson, J. Lee, N. A. Kotov, *Nanoscale Res. Lett.* **2006**, *1*, 84; b) A. O. Govorov, H. H. Richardson, *Nano Today* **2007**, *2*, 30.
- [20] S. Freddi, L. Sironi, R. D'Antuono, D. Morone, A. Doná, E. Cabrini, L. D'Alfonso, M. Collini, P. Pallavicini, G. Baldi, *Nano Lett.* **2013**, *13*, 2004.
- [21] G. Palermo, L. D. Sio, T. Placido, R. Comparelli, M. L. Curri, R. Bartolino, C. Umeton, *Mol. Cryst. Liq. Cryst.* **2015**, *614*, 93.
- [22] L. De Sio, G. Caracciolo, F. Annesi, T. Placido, D. Pozzi, R. Comparelli, A. Pane, M. L. Curri, A. Agostiano, R. Bartolino, *Micro Nano Syst. Lett.* **2015**, *3*, 8.
- [23] A. Samadi, H. Klingberg, L. Jauffred, A. Kjær, P. M. Bendix, L. B. Oddershede, *Nanoscale* **2018**, *10*, 9097.
- [24] M. Born, E. Wolf, *Principles Of Optics: Electromagnetic Theory Of Propagation, Interference And Diffraction Of Light*, Elsevier, Amsterdam **2013**.
- [25] a) C. F. Bohren, D. R. Huffman, *Absorption and Scattering of Light by Small Particles*, John Wiley & Sons, Hoboken, NJ **2008**; b) *Active Plasmonic Nanomaterials* (L. De Sio), CRC Press, Boca Raton, FL **2015**; c) H. Horvath, *J. Quant. Spectrosc. Radiat. Transfer* **2009**, *110*, 787.
- [26] B. Palpant, in *Gold Nanoparticles For Physics, Chemistry And Biology*, **2012**, p. 75.
- [27] G. Baffou, in *Thermoplasmonics: Heating Metal Nanoparticles Using Light*, Cambridge University Press, Cambridge, UK **2017**.
- [28] M. Kim, J. H. Lee, J. M. Nam, *Adv. Sci.* **2019**, *6*, 1900471.
- [29] G. Baffou, R. Quidant, *Laser Photon. Rev.* **2013**, *7*, 171.
- [30] V. Amendola, R. Pilot, M. Frascioni, O. M. Maragò, M. A. Iatì, *J. Phys.: Condens. Matter* **2017**, *29*, 203002.
- [31] L. Jauffred, A. Samadi, H. Klingberg, P. M. Bendix, L. B. Oddershede, *Chem. Rev.* **2019**, *119*, 8087.
- [32] G. Baffou, R. Quidant, F. J. García de Abajo, *ACS Nano* **2010**, *4*, 709.
- [33] L. Pezzi, L. De Sio, A. Veltri, T. Placido, G. Palermo, R. Comparelli, M. L. Curri, A. Agostiano, N. Tabiryan, C. Umeton, *Phys. Chem. Chem. Phys.* **2015**, *17*, 20281.
- [34] G. Baffou, P. Berto, E. Bermúdez Ureña, R. Quidant, S. Monneret, J. Polleux, H. Rigneault, *ACS Nano* **2013**, *7*, 6478.
- [35] L. Pezzi, G. Palermo, A. Veltri, U. Cataldi, T. Bürgi, T. Ritacco, M. Giocondo, C. Umeton, A. De Luca, *J. Phys. D: Appl. Phys.* **2017**, *50*, 435302.
- [36] a) J.-T. Lin, Y.-L. Hong, C.-L. Chang, presented at *Optical Interactions with Tissues and Cells XXI. International Society for Optics and Photonics. Event: SPIE BiOS*, San Francisco, CA, USA, Vol. 7562 **2010**, p. 75620R; b) K. Yue, J. Nan, X. Zhang, J. Tang, X. Zhang, *Appl. Therm. Eng.* **2016**, *99*, 1093; c) R. Carrillo-Torres, M. García-Soto, S. Morales-Chávez, A. Garibay-Escobar, J. Hernández-Paredes, R. Guzman, M. Barboza-Flores, M. Álvarez-Ramos, *RSC Adv.* **2016**, *6*, 41304.
- [37] a) S. Maity, W.-C. Wu, J. B. Tracy, L. I. Clarke, J. R. Bochinski, *Nanoscale* **2017**, *9*, 11605; b) M.-J. Chiu, L.-K. Chu, *Phys. Chem. Chem. Phys.* **2015**, *17*, 17090.
- [38] A. T. Luk, F. Nouizi, M. Marks, T. Kart, G. Gulsen, presented at *Optical Interactions with Tissue and Cells XXVII. International Society for Optics and Photonics. Event: SPIE BiOS* San Francisco, CA, USA, Vol. 9706, **2016**, p. 97060M.
- [39] O. Nakabeppu, M. Chandrachood, Y. Wu, J. Lai, A. Majumdar, *Appl. Phys. Lett.* **1995**, *66*, 694.
- [40] a) Y. Wang, K. C. Black, H. Luehmann, W. Li, Y. Zhang, X. Cai, D. Wan, S.-Y. Liu, M. Li, P. Kim, *ACS Nano* **2013**, *7*, 2068; b) G. Chernov, J. Ibarra-Valdez, R. Carrillo-Torres, T. Medrano-Pesqueira, V. Chernov, M. Barboza-Flores, *Plasmonics* **2019**, *14*, 935; c) K. A. López-Varela, N. Cayetano-Castro, E. S. Kolosovas-Machuca, F. J. Gonzalez, F. S. Chiwo, J. L. Rodríguez-López, *J. Nanomater.* **2018**, 2018.
- [41] Z. Ioffe, T. Shamai, A. Ophir, G. Noy, I. Yutsis, K. Kfir, O. Cheshnovsky, Y. Selzer, *Nat. Nanotechnol.* **2008**, *3*, 727.
- [42] a) L. Gao, L. Wang, C. Li, Y. Liu, H. Ke, C. Zhang, L. V. Wang, *J. Biomed. Opt.* **2013**, *18*, 026003; b) L. Gao, C. Zhang, C. Li, L. V. Wang, *Appl. Phys. Lett.* **2013**, *102*, 193705.
- [43] G. Baffou, M. Kreuzer, F. Kulzer, R. Quidant, *Opt. Express* **2009**, *17*, 3291.
- [44] L. De Sio, T. Placido, S. Serak, R. Comparelli, M. Tamborra, N. Tabiryan, M. L. Curri, R. Bartolino, C. Umeton, T. Bunning, *Adv. Opt. Mater.* **2013**, *1*, 899.
- [45] G. Huttmann, R. Birngruber, *IEEE J. Sel. Top. Quantum Electron.* **1999**, *5*, 954.
- [46] C. Hrelescu, J. Stehr, M. Ringler, R. A. Sperling, W. J. Parak, T. A. Klar, J. Feldmann, *J. Phys. Chem. C* **2010**, *114*, 7401.
- [47] a) A. Urban, M. Fedoruk, M. Horton, J. Radler, F. D. Stefani, J. Feldmann, *Nano Lett.* **2009**, *9*, 2903; b) A. Kyrsting, P. M. Bendix, D. G. Stamou, L. B. Oddershede, *Nano Lett.* **2011**, *11*, 888.
- [48] a) M. Zhu, G. Baffou, N. Meyerbröcker, J. Polleux, *ACS Nano* **2012**, *6*, 7227; b) A. Bahadori, L. B. Oddershede, P. M. Bendix, *Nano Res.* **2017**, *10*, 2034.
- [49] D. Jaque, L. M. Maestro, B. Del Rosal, P. Haro-Gonzalez, A. Benayas, J. Plaza, E. M. Rodriguez, J. G. Sole, *Nanoscale* **2014**, *6*, 9494.
- [50] A. B. Flir, *The Ultimate Infrared Handbook for R&D Professionals FLIR Systems*, Boston **2010**. pp. 1–39.
- [51] P. Tavakolian, A. Mandelis, *J. Appl. Phys.* **2018**, *124*, 160903.
- [52] a) S. Ranjit, M. Choi, W. Kim, *J. Mech. Sci. Technol.* **2016**, *30*, 1111; b) S. S. Pawar, V. P. Vavilov, *Int. J. Heat Mass Transfer* **2016**, *94*, 56.
- [53] D. Gavrilov, R. G. Maev, D. Almond, *Can. J. Phys.* **2014**, *92*, 341.
- [54] C. L. West, A. C. Doughty, K. Liu, W. R. Chen, *J. Bio-X Res.* **2019**, *2*, 159.
- [55] Y. Okano, K. Ito, I. Ida, M. Takahashi, *IEEE Trans. Microwave Theory Tech.* **2000**, *48*, 2094.
- [56] L. M. Blinov, in *Electro-Optical and Magneto-Optical Properties of Liquid Crystals* (Ed: L. M. Blinov), John Wiley & Sons, Inc., New York, NY, USA **1983**, p. 212.
- [57] P. G. de Gennes, J. Prost, *The Physics of Liquid Crystals*, Vol. 83, Oxford University press, Oxford, UK **1993**.
- [58] U. A. Hrozhyk, S. V. Serak, N. V. Tabiryan, L. Hoke, D. M. Steeves, B. R. Kimball, *Opt. Express* **2010**, *18*, 8697.
- [59] a) H. H. Richardson, Z. N. Hickman, A. O. Govorov, A. C. Thomas, W. Zhang, M. E. Kordesch, *Nano Lett.* **2006**, *6*, 783; b) O. M. Wilson, X. Hu, D. G. Cahill, P. V. Braun, *Phys. Rev. B* **2002**, *66*, 224301; c) J. Lee, A. O. Govorov, N. A. Kotov, *Angew. Chem. Int. Ed. Engl.* **2005**, *44*, 7439.
- [60] X. Huang, S. Neretina, M. A. El-Sayed, *Adv. Mater.* **2009**, *21*, 4880.
- [61] H. Finkelmann, S. T. Kim, A. Muñoz, P. Palffy-Muhoray, B. Taheri, *Adv. Mater.* **2001**, *13*, 1069.
- [62] L. De Sio, U. Cataldi, A. Guglielmelli, T. Bürgi, N. Tabiryan, T. J. Bunning, *MRS Commun.* **2018**, *8*, 550.
- [63] S. Kim, A. N. Mitropoulos, J. D. Spitzberg, H. Tao, D. L. Kaplan, F. G. Omenetto, *Nat. Photonics* **2012**, *6*, 818.
- [64] R. M. Gazoni, M. G. Bellino, M. Cecilia Fuertes, G. Giménez, G. J. A. A. Soler-Illia, M. L. M. Ricci, *J. Mater. Chem. C* **2017**, *5*, 3445.
- [65] L. De Sio, P. F. Lloyd, N. V. Tabiryan, T. Placido, R. Comparelli, M. L. Curri, T. J. Bunning, *ACS Appl. Nano Mater.* **2019**, *2*, 3315.
- [66] L. De Sio, P. F. Lloyd, N. V. Tabiryan, T. J. Bunning, *ACS Appl. Mater. Interfaces* **2018**, *10*, 13107.

- [67] P. W. Zhu, D. H. Napper, *J. Colloid Interface Sci.* **1996**, *177*, 343.
- [68] L. D. Carlos, F. Palacio, *Thermometry At The Nanoscale: Techniques and Selected Applications* (Eds: L. D. Carlos, F. Palacio), Royal Society of Chemistry, London, UK Vol. 38, **2016**.
- [69] Y. Guan, Y. Zhang, *Soft Matter* **2011**, *7*, 6375.
- [70] K. Matsumoto, N. Sakikawa, T. Miyata, *Nat. Commun.* **2018**, *9*, 1.
- [71] F. Pierini, P. Nakielski, O. Urbanek, S. Pawłowska, M. Lanzi, L. De Sio, T. A. Kowalewski, *Biomacromolecules* **2018**, *19*, 4147.
- [72] Z. Zhang, J. Wang, X. Nie, T. Wen, Y. Ji, X. Wu, Y. Zhao, C. Chen, *J. Am. Chem. Soc.* **2014**, *136*, 7317.
- [73] A. Saeed, D. M. Georget, A. G. Mayes, *J. Polym. Sci., Part A: Polym. Chem.* **2010**, *48*, 5848.
- [74] M. Wei, M. J. Serpe, *Part. Part. Syst. Charact.* **2019**, *36*, 1800326.
- [75] J. E. Cho, S. Kim, S. Son, J. Yang, M. S. Kang, S. H. Eom, S. C. Yoon, M. H. Kim, B. Kim, *J. Phys. Chem. C* **2019**, *123*, 2755.
- [76] Y. Shi, C. Ma, L. Peng, G. Yu, *Adv. Funct. Mater.* **2015**, *25*, 1219.
- [77] S. Shi, L. Zhang, T. Wang, Q. Wang, Y. Gao, N. Wang, *Soft Matter* **2013**, *9*, 10966.
- [78] B. Mutharani, P. Ranganathan, S.-M. Chen, *Sens. Actuators B: Chem.* **2020**, *304*, 127232.
- [79] Z. H. Farooqi, S. R. Khan, R. Begum, A. Ijaz, *Rev. Chem. Eng.* **2016**, *32*, 49.
- [80] F. Pierini, A. Guglielmelli, O. Urbanek, P. Nakielski, L. Pezzi, R. Buda, M. Lanzi, T. A. Kowalewski, L. De Sio, *Adv. Opt. Mater.* **2020**, 2000324.
- [81] Á. Artiga, S. García-Embú, L. De Matteis, S. G. Mitchell, J. M. de la Fuente, *Front. Chem.* **2018**, *6*.
- [82] N. Pourreza, M. Ghomi, *Microchim. Acta* **2020**, *187*, 133.
- [83] J. Song, S. Hwang, K. Im, J. Hur, J. Nam, S. Hwang, G. O. Ahn, S. Kim, N. Park, *J. Mater. Chem. B* **2015**, *3*, 1537.
- [84] B. Miranda, R. Moretta, S. D. Martino, P. Dardano, I. Rea, C. Forestiere, L. D. Stefano, *J. Appl. Phys.* **2021**, *129*, 033101.
- [85] P. Nakielski, S. Pawłowska, C. Rinoldi, Y. Ziai, L. De Sio, O. Urbanek, K. Zembrzycki, M. Pruchniewski, M. Lanzi, E. Salatelli, *ACS Appl. Mater. Interfaces* **2020**.
- [86] J. Zeng, D. Shi, Y. Gu, T. Kaneko, L. Zhang, H. Zhang, D. Kaneko, M. Chen, *Biomacromol.* **2019**, *20*, 3375.
- [87] J. Lin, Z. He, F. Liu, J. Feng, C. Huang, X. Sun, H. Deng, *Int. J. Nanomed.* **2020**, *15*, 5377.
- [88] L. De Sio, B. Ding, M. Focsan, K. Kogermann, P. Pascoal-Faria, F. Petronella, G. Mitchell, E. Zussman, F. Pierini, *Chemistry* **2021**, *27*, 6112.



Alexa Guglielmelli received her B.S. in physics and M.S. in molecular biophysics from University of Calabria, Cosenza, Italy (UNICAL). She received the Ph.D in physical, chemical, and materials sciences and technologies from the same university. Her research interests include plasmonic nanomaterials for applications in nanomedicine and biophotonics and thermotropic liquid crystals applications.



Filippo Pierini is a professor and the Pierini Research Group head at the Institute of Fundamental Technological Research (IPPT PAN). He received his M.Sc. in advanced chemical methodologies with the highest marks and honors (110/110 summa cum laude) in 2009, and Ph.D. in chemical sciences at the University of Bologna (Italy) in 2013. His research interests include light-matter interaction, stimuli-responsive hydrogel, and the development of functional fibrous nanomaterials.



Nelson Tabiryan pioneered development of the fourth generation optics technology—diffractive waveplates—marking a major breakthrough in planar optics. He is the CEO of Beam Engineering for Advanced Measurements Corporation that demonstrated the thinnest and largest spectrally and angularly broadband planar optical components. He received a Ph.D. degree in physics and mathematics in 1982 and D.Sc. degree in 1986. He is an OSA fellow, NIAC fellow, Alexander Von Humboldt research scholar, recipient of the Frederiks Medal, and the American Chemical Society's Cooperative Research Award (2013). He has over 250 refereed publications and 50 issued patents.



Cesare P. Umeton has been researcher, associate professor and full professor of experimental physics at the Physics Department, University of Calabria, where he has been also president of the “Degree Course in Materials Science” and coordinator of the “Optics Group.” He is an OSA fellow, president of the association “Novel Optical Materials and Applications.” In the field of atomic and molecular physics and optics of liquid crystalline composite materials, he has been manager of several international projects and is coauthor of more than 180 articles in international journals and more than 170 communications at international conferences.



Timothy J. Bunning is the chief technology officer for Air Force Research Laboratory (AFRL). He serves as the corporate-level S&T interface for a government workforce of ~6000 people in the laboratory’s nine technology directorates and 711th Human Performance Wing. He is active in numerous technical communities and is a fellow of AFRL, OSA, SPIE, APS, ACS, RSC, and MRS. He has coauthored more than 300 refereed papers and holds 18 patents. He is an adjunct professor in the Department of Materials Science and Engineering, Georgia Institute of Technology and is in the editorial boards of several materials-centric journals.



Luciano De Sio works at the Sapienza University of Rome. He is the group leader of a young and highly motivated research group working in thermoplasmonics, liquid crystals, nanotechnology, optics, and biophotonics. He has co-authored 110 ISI-JCR publications in physics and biomedicine, several book chapters, 18 issued international patents, and delivered more than 50 scientific communications at conferences. He is also the project director of an international Multi-Year Project supported by the NATO Science for Peace and Security Program, aiming to realize a nanotechnology-inspired biosensor with photo-responsive liquid crystals.